

JGR Space Physics

RESEARCH ARTICLE

10.1029/2022JA030635

Key Points:

- O⁺ flux tends to respond more strongly to energy inputs than H⁺ flux
- The lower bound of the ion flux at 4,000 km is typically defined by the polar wind H⁺ except when large e⁻ precipitation is present
- The peak response of the outflow to energy input can be different than the steady state response

Correspondence to:

A. Glocer,
alex.glocer-1@nasa.gov

Citation:

Glocer, A., & Daldorff, L. K. S. (2022). Connecting energy input with ionospheric upflow and outflow. *Journal of Geophysical Research: Space Physics*, 127, e2022JA030635. <https://doi.org/10.1029/2022JA030635>

Received 7 MAY 2022

Accepted 16 AUG 2022

Author Contributions:

Conceptualization: A. Glocer
Data curation: L. K. S. Daldorff
Formal analysis: L. K. S. Daldorff
Funding acquisition: A. Glocer
Investigation: A. Glocer, L. K. S. Daldorff
Methodology: A. Glocer, L. K. S. Daldorff
Project Administration: A. Glocer
Resources: A. Glocer
Software: A. Glocer, L. K. S. Daldorff
Validation: L. K. S. Daldorff
Visualization: L. K. S. Daldorff
Writing – original draft: A. Glocer
Writing – review & editing: A. Glocer, L. K. S. Daldorff

© 2022 The Authors. This article has been contributed to by U.S. Government employees and their work is in the public domain in the USA.

This is an open access article under the terms of the Creative Commons Attribution-NonCommercial-NoDerivs License, which permits use and distribution in any medium, provided the original work is properly cited, the use is non-commercial and no modifications or adaptations are made.

Connecting Energy Input With Ionospheric Upflow and Outflow

A. Glocer¹  and L. K. S. Daldorff^{1,2} 

¹NASA/GSFC, Greenbelt, MD, USA, ²Catholic University of America, Washington, DC, USA

Abstract The connection between energy inputs and the generation of ion upflows and outflows is a topic of keen scientific interest and the subject of a number of empirical studies. Despite this interest, it remains uncertain how different ion species respond to energy input, what defines the upper and lower bounds of the ion flux, and what role solar illumination plays in regulating the relationship between energy input and ion upflows/outflows. This work simulates how ion flux scales with low and high altitude energization, and to a combination of both. Furthermore, we examine the influence of solar illumination on these relationships by considering how the scaling of ion flux with energy input changes over the solar cycle, comparing solar minimum and maximum, as well as how they change from day to night conditions. We find O⁺ flux tends to respond more strongly to energy inputs than H⁺ flux, with the O⁺ flux often exhibiting a lower activation energy and a greater dynamic range. The lower bound of the ion flux at 4,000 km is typically defined by the polar wind H⁺, although O⁺ upflows can dominate at low altitudes in the presence of significant frictional heating of the ion gas or soft electron precipitation. However, when significant soft electron precipitation and wave-particle interactions are present simultaneously the lower bound of the ion flux at 4,000 km is defined by the O⁺. Finally, we find a difference between the steady state response of the outflow to energy input and the peak response.

1. Introduction

The transport of ions from the ionosphere and into the magnetosphere, known as “ionospheric outflow” or “ion outflow,” has many implications for Earth’s magnetospheric composition and dynamics. Plasma in the magnetosphere resulting from ionospheric outflow is found to alter magnetic reconnection (e.g., Karimabadi et al., 2011; Shay et al., 2004), change the flows in the magnetotail (e.g., Brambles et al., 2011; Garcia et al., 2010), and impact the inner magnetosphere (e.g., Moore et al., 2005; Welling et al., 2011). Moreover, the ionosphere is at times found to be a dominant source of magnetospheric plasma, particularly during geomagnetic storms (Lennartsson et al., 1981) and is arguably a fully adequate source of near-Earth plasma (Chappell et al., 1987; Huddleston et al., 2005). Given the importance of ion outflow to the magnetosphere, it is critical to understand how energy input to the ionosphere drives ionospheric outflow.

Energy input in the form of electromagnetic energy and particle precipitation has been shown in observations to be associated with the generation of ion outflows. In particular, statistical studies using data from the POLAR spacecraft (Zheng et al., 2005) and the Fast Auroral Snapshot (FAST) spacecraft (Strangeway et al., 2005) found a strong correlation between ion outflow flux, Poynting flux, and soft electron precipitation. In these studies, energy inputs and ion outflows were compared at high altitudes, far above the source region of the ion escape. Earlier observations from the Dynamics Explorer (DE) 2 spacecraft also found a connection between soft electron precipitation and ion upflows above the aurora (Seo et al., 1997). Interestingly, the studies of Zheng et al. (2005) and Strangeway et al. (2005) focus on the DC, or quasi-static, Poynting flux. The DC Poynting flux is associated with the large scale convection which can influence ion outflow by generating ion upwelling driven by frictional heating of the ion gas. While much of this heating occurs in the *E*-region, large amounts are also possible in the *F*-region (Killeen & Roble, 1984) which can then generate significant transient ion upwelling in the cusp and auroral regions (Gombosi & Killeen, 1987). Similarly, soft electron precipitation can heat the thermal electron population and generate secondary electrons which can enhance the ambipolar electric field and thus lift ionospheric plasma to higher altitudes (Su et al., 1999). The upwelling of plasma caused by either of these processes was speculated by Strangeway et al. (2005) as the first step of the causal chain explaining ion outflow with subsequent wave-particle interactions (WPI) being required to further accelerate the ions to create the energized outflow observed by FAST and POLAR. The online supplemental materials for Brambles et al. (2011) expands

on this picture by looking at the correlation between ion outflow and the low frequency Alfvénic Poynting flux (bandpass filtered for 5–180 s), finding a strong correlation.

An important process that may be responsible for the creation of energetic ion outflows at high altitudes is the ion cyclotron resonant heating (ICRH) mechanism described theoretically by Chang et al. (1986) and Crew et al. (1990). In this mechanism, ions interact resonantly with a portion of the broad-band turbulent wave spectrum which is near the ion cyclotron frequency. As a result of this interaction, the ion distribution function will heat perpendicularly to the magnetic field. The mirror force is then able to accelerate ions parallel to the field. Such heating events were found by a survey of observations by the Freja satellite to be the most frequent type observed (André et al., 1998).

In addition to the ICRH mechanism mentioned above, there are a number of other WPI that are thought to play a role in the generation of ion outflow. For instance, interactions with lower hybrid waves excited in the auroral regions are able to scatter particles above the thermal velocity and contribute to the formation of high energy tails in the outflowing distribution (e.g., Chang & Coppi, 1981; Rettner et al., 1994). Interaction of particles with dispersive Alfvén waves are also thought to be an important processes for accelerating ions. In this mechanism ions undergo stochastic heating when passing through the perpendicular electric field of an oblique wave with a wavelength that approaches the gyroradius of the particle (Chaston et al., 2004). FAST observations found that a sizable fraction (15%–34%) of energetic outflows may be associated with this mechanism (Chaston et al., 2007).

Recently, Zhao et al. (2020) revisited the analysis of the FAST observations of ion outflow above the cusp to evaluate effectiveness of energy inputs in driving outflow for O⁺ and H⁺ ions separately. They found that the correlations are different between energy inputs and O⁺ and H⁺ outflows with O⁺ outflows correlating best with DC Poynting flux and H⁺ outflows correlating best with soft electron precipitation. Additionally, they found that O⁺ tends to respond more strongly to energy inputs than H⁺ does. The causes underlying the different response of ion species to energy inputs requires further investigation.

First principles models of ion outflow have been used to better understand the observed correlation between energy inputs and the generation of ion outflows. For instance, Su et al. (1999) used the Field Line Interhemispheric Plasma model described by Richards and Torr (1986) to investigate the connection between soft electron precipitation and ion upwelling. Their modeling results found that ion upflow velocity and electron temperature is strongly connected with soft electron precipitation. These connections supported the idea that thermal electron heating through interactions with soft electron precipitation in the topside *F*-region serve to heat and lift the plasma. Moreover, Su et al. (1999) also found that lower energy electron precipitation (below 100 eV) at a given energy flux tends to be more effective in generating ion upflows than higher energy precipitation. This is because lower characteristic energy precipitation deposits more of its energy in the topside ionosphere, while higher energy precipitation penetrates too deeply into the atmosphere to be highly effective in the generation of ion outflows. The effect of both soft electron precipitation and WPI via the ICRH mechanism was also systematically examined by Zeng and Horwitz (2007) using the Dynamic Fluid-Kinetic model which has a fluid solution at low altitudes and a kinetic hybrid-PIC representation at high altitudes. In this study they simulated the outflow along a particular dayside field line with a specified level of solar flux ($F10.7 = 142$) and geomagnetic activity ($AP = 17$). The energy inputs in the form of precipitation and wave power spectral density were then swept over multiple simulations. From these simulations they found a relationship for the O⁺ flux accounting for both precipitating electron flux and wave power. Zeng and Horwitz (2007) also interestingly found what they call a “valve” effect, in which the waves act to regulate the amount of energized O⁺ outflows. In other words, they found that there is a minimum threshold for the waves to be effective in generating heating. They further found that beyond a certain level of wave input the flux of O⁺ saturates.

This past work has helped to improve our understanding of the causal drivers that underlie the observed correlation between energy input and outflow, but a number of open issue remain. For instance, both the observations and simulation studies indicate that the outflow flux will saturate beyond some level of energy input, but what controls the saturation flux and how the saturation flux differs by species remains unknown. Additionally, the observational studies described above are based on a very limited number of events and focus largely on the dayside. It is highly likely that the relationship between energy input and outflow is affected by illumination, but just how the relationship can change requires further study. For instance, a very recent study using FAST data shows that the strongest outflow events tend to be observed on the dayside, which highlights the potential

importance of illumination which should be further examined (Kitamura et al., 2021). It should not, in general, be expected that outflow will respond in the same way at solar maximum and solar minimum, or in the dayside cusp and nightside auroral region. Finally, it was noted in Strangeway et al. (2005) and Zhao et al. (2020) that many parameters in the dayside cusp are correlated and it is therefore difficult to separate how different physical mechanisms can be contributing to the final relationship between outflow flux and energy input.

In this study we use numerical simulations to address the issues described in the previous paragraph. In Section 2 we briefly describe the model used in this study as well as the study setup and the motivation for the different simulations conducted. The results are presented in Section 3. Finally, conclusions and further discussion are provided in Section 4.

2. Modeling Approach and Methodology

In this section we provide a brief overview of the model used for the outflow simulations in this study as well as the approach to selecting the simulations and conducting the analysis.

2.1. Modeling the Outflow Response to Energy Input

In this study we use the Polar Wind Outflow Model (PWOM) (Glocer et al., 2007, 2009) in order to simulate the response of ion outflow to energy input under various conditions. PWOM provides a first principles solution of the transport of plasma from the F-region of the ionosphere to the magnetosphere for H⁺, O⁺, He⁺, and electrons. Although recent work has added N⁺ and some molecular ions to a version of PWOM (Lin et al., 2020), these additional species are not considered in the present study. At low altitudes, below 1,000 km, the model solves the gyrotrropic transport equations for each ion fluid (Gombosi & Nagy, 1989). At high altitudes, above 1,000 km, the model switches to a hybrid PIC approach and follows the gyroaveraged particle equation of motion including collisions with a Monte Carlo approach. The ions are solved in a static neutral background provided by the empirical MSIS model (Picone, 2002). A comprehensive description of PWOM was published recently by Glocer et al. (2018) and interested readers are referred to that work for complete details. Instead, we will focus on providing a brief description of how PWOM captures the energy inputs which are the focus of this study.

To capture WPI responsible for transverse heating of ions at high altitudes, PWOM applies a series of perpendicular velocity perturbations to the macro particles in the wave heating region that mimic the stochastic wave heating process. The distribution of velocity perturbations are randomly chosen to conform to D_{\perp} which is the quasi-linear diffusion coefficient for diffusion perpendicular to the magnetic field. In past studies, we chose an empirical specification for this term put forward by Barakat and Schunk (2001). However, in the present study we instead adopt the specification of Crew et al. (1990) which is given as follows:

$$D_{\perp} = (\pi q^2 / 2m_i^2) |E_L|^2(\Omega(s)) \quad (1)$$

where q is the charge, m_i is the ion mass, $\Omega(s)$ is the gyro-frequency at position s , and $|E_L|^2$ is the left hand polarized portion of the electric field spectral density. By assuming that the electric field spectral density has a power law form with a spectral index α and frequency ω such that $|E_L|^2(\omega) \propto \omega^{-\alpha}$, and accounting for the variation of the cyclotron frequency with radius in a dipole field, Crew et al. (1990) arrives at the following simplified expression:

$$D_{\perp} = (\eta q^2 / 4m_i^2) |E_o|^2 \left(\frac{r}{r_o} \right)^{3\alpha} \quad (2)$$

where η is the fraction of waves with left hand polarization, $|E_o|^2$ is the electric field spectral density at a reference radial distance r_o , and at frequency the cyclotron frequency at that reference location. The diffusion coefficient in this form is highly convenient as it does not depend on velocity and can be fully specified by the power spectral density at a given altitude. Note that inherent to this formula is the assumption that the wave spectrum is constant in altitude.

To capture the effects of soft electron precipitation, and superthermal electrons in general, PWOM includes multiple treatments of energetic electron transport. These include a fully kinetic solution of the superthermal electrons (Glocer et al., 2017), as well as a two-stream representation (Glocer et al., 2018) using a adapted version

of the GLOW code (Solomon, 2017; Solomon et al., 1988). In both cases the energetic electrons feedback to the outflow solution through enhanced ion production, thermal electron heating, as well as through the currentless condition (e.g., Khazanov et al., 1997). As a result of all these changes, the ambipolar electric field is enhanced which in turn impacts the ion evolution. For this study we use the GLOW two-stream treatment for the superthermal electrons as it provides a sufficiently physical treatment at a reduced computational expense. For this calculation the precipitating electron spectrum is imposed using the following spectrum (Rees, 1989):

$$\Phi_b(E) = AE e^{-E/E_o} \quad (3)$$

where $\Phi_b(E)$ is the precipitation electron flux imposed on the upper boundary of the downward stream, E_o is the characteristic energy, and A is a normalization factor to ensure the desired energy flux.

Frictional heating of the ion gas is included in the model by way of a source term in the energy equation (Schunk & Nagy, 2000):

$$\frac{\delta E_i}{\delta t} = \sum_n \frac{\rho_i \nu_{in}}{m_i + m_n} [m_n (u_{i\perp} - u_{n\perp})^2] \quad (4)$$

where ν_{in} is the ion neutral collision frequency, ρ_i is the ion mass density, m_n is neutral mass, and $u_{i\perp}$ and $u_{n\perp}$ are the ion and neutral velocities perpendicular to the local magnetic field. Note that the sum is only over neutrals as we are specifically calling out the contribution of frictional heating on a particular ion species “i” due to the difference in perpendicular motion relative to the neutrals. As you can see, this term represents the friction heating due to the differential motion of ion and neutral fluids.

While other outflow mechanisms may be at work, the present study focuses on WPI through ICRH with broad band electromagnetic low frequency (BBELF) waves, and the consequences of soft electron precipitation and frictional heating of the ions. For more details of the PWOM code used in this study we refer the reader back to Glocer et al. (2018).

2.2. Simulation Methodology

Our goal in this study is to examine the efficiency of converting input energy into ion upwelling and outflow for different mechanisms under a variety of conditions. With this objective in mind, we use the empirical paradigm discussed by Strangeway et al. (2005) to provide a roadmap to focus our simulation effort. In particular, that study inferred low altitude upwelling mechanisms associated with the two observed energy inputs from soft electron precipitation and frictional heating of the ions. The supposition was that these energy inputs deposit energy at low altitudes and lifts the plasma to higher altitudes where transverse heating driven by WPI can take over and supply the remaining energy required to let ions escape. We align our simulation effort with these three energy inputs in order to understand the contribution from each. The following paragraphs further detail the simulation configuration.

For each energy input, we consider the resulting ion flux as we sweep the input value. In particular, we define a maximum and minimum input value and conduct a sequence of 20 simulations spanning the defined range. For dayside simulations, each sweep over a given parameter starts from a steady state solution representing the plasma on an open field line at a magnetic latitude of 70° exposed only to solar EUV input. The energy input being examined in a given simulation sweep switches on at time 0 and the simulation continues for 20 min. This set up reasonably mimics a convecting field line initially exposed only to solar EUV input which suddenly encounters the cusp.

We further examine how solar EUV flux impacts the connection between energy inputs and upflowing ion flux. Two types of EUV flux changes are considered: (a) solar max versus solar min, and (b) day versus night. For the first case, we consider two values of F10.7 representing solar maximum (180) and solar minimum (80). These values of F10.7 are used to set the solar EUV spectrum used in the calculation of the photoionization rate, the photoelectron calculation, and also sets the background empirical neutral thermosphere profile. The specified value of F10.7 is used for both obtaining the steady state initial condition as well as the portion of the run after the energy input of interest is switched on. Day-night illumination differences are the second way that solar EUV flux can alter the connection between energy inputs and upflowing ion flux. For the nightside field line we start with

the dayside initial condition and place it on the nightside at the same latitude. New nightside initial conditions are obtained by running the simulation for convection times representing the time for a field line starting on the dayside to reach this location on the nightside. The speed of convection is important to the nightside initial condition as it affects how much the flux tube depletes as it moves from illuminated to non-illuminated conditions.

It is important to note that considering all possible combinations of energy inputs and conditions requires an extreme number of simulations and is therefore beyond the scope of the present work. However, we do consider the scaling of ion upflow/outflow with each energy inputs under different solar flux conditions on the dayside. We explore how the effectiveness of wave-heating is different in the dayside cusp versus the nightside auroral region. Additionally, we consider a limited number of combinations to illustrate how scaling relationships between energy input and ion upflow/outflow change when different energy inputs occur simultaneously.

3. Results

3.1. Ion Flux Scaling With Frictional Heating of the Ion Gas

Regions of strong convection can potentially deposit significant frictional heating in the topside ionosphere. In particular, the portion of this heating deposited in the *F*-region can be particularly effective at generating significant transient upwelling of ions. As indicated by Equation 4, this heating is due to the differential motion of the ions and neutrals. It is interesting to note that Joule heating, the frictional heating rate of the total (ion and neutral) gas, is related to the frictional heating of the ion gas by a factor of $m_n/(m_i + m_n)$ (Strangeway, 2012). Some prior studies have looked at the relationship between ion upflow and Joule heating, but we focus particularly on the frictional heating of the ion gas as the more relevant quantity in looking at ion upflow. In this section we will conduct a series of simulations to examine the connection between ion upflows and increasing ion convection velocity in the sunlit high latitude region. In these simulations, we vary the magnitude of the difference between the ion and neutral velocity perpendicular to the magnetic field ($|u_{i\perp} - u_{n\perp}|$) and look at the ion flux parallel to the magnetic field at two altitudes located at the top of the exobase transition region (1,200 km) and at nominal FAST satellite altitudes (4,000 km) where previous empirical studies were carried out.

Figure 1 presents the results of the simulations showing how the up flowing ion flux varies with $V_c = |u_{i\perp} - u_{n\perp}|$. The peak flux associated with this transient up welling does not occur at the same time for each value of V_c . Therefore, in our results we plot the peak flux for each value of V_c rather than the value at a fixed time. Each panel shows V_c on the *x*-axis and log of the ion flux on the *y*-axis. The O⁺ flux is shown in blue while the H⁺ flux is shown in red. The top row of the figure presents the solution for solar max while the bottom row shows the result for solar min. Additionally, the left column shows the result at 1,200 km while the right column shows the result at 4,000 km. It should be noted that a region of enhanced frictional heating of the ions creates a transient bulge of up flowing ions (Gombosi & Killeen, 1987) which makes focusing on the peak ion flux particularly important.

A number of observations can be drawn from results in Figure 1. First, there is a minimum threshold of V_c to trigger an ion upflow response. That minimum threshold is different for H⁺ and O⁺ with O⁺ exhibiting a response at lower values of V_c than H⁺. Second, the O⁺ flux responds more strongly to frictional heating energy inputs than H⁺. It not only responds more to lower energy inputs, but it has larger peak flux values and the power law slope indicated on the plot is steeper indicating a stronger response to increasing energy input. Third, not all of the O⁺ flowing up at 1,200 km will reach 4,000 km while much more of the enhanced H⁺ flux will reach 4,000 km. Additionally, the power law response of the ion flux becomes much steeper at higher altitudes with very little O⁺ up flowing for energy inputs below $V_c = 1$ km/s. One implication of these results is that frictional heating can loft O⁺ from low altitudes to very high altitudes with a dependence on the level of energy input, but additional acceleration processes are required to get the O⁺ out to the magnetosphere. Therefore, frictional heating can be quite effective at lifting a large amount of O⁺ which can then feed into the wave-heating at high altitudes.

Figure 1 also lets us examine how the effectiveness of converting frictional heating of the ions into ion upflow varies with solar illumination. In general, we find that the maximum flux of ions that can be lifted during solar maximum conditions is greater than the maximum flux of ions during solar minimum as there is simply more ions available due to enhanced photoionization. However, at 1,200 km altitude the power law dependence of the ion flux on energy input is found to be similar. At 4,000 km the trend is also found to be similar between solar max and solar min simulations, although the power law is somewhat different. The solar illumination therefore is seen to have a larger effect on the flux magnitude than on the general trend connecting ion flux and V_c .

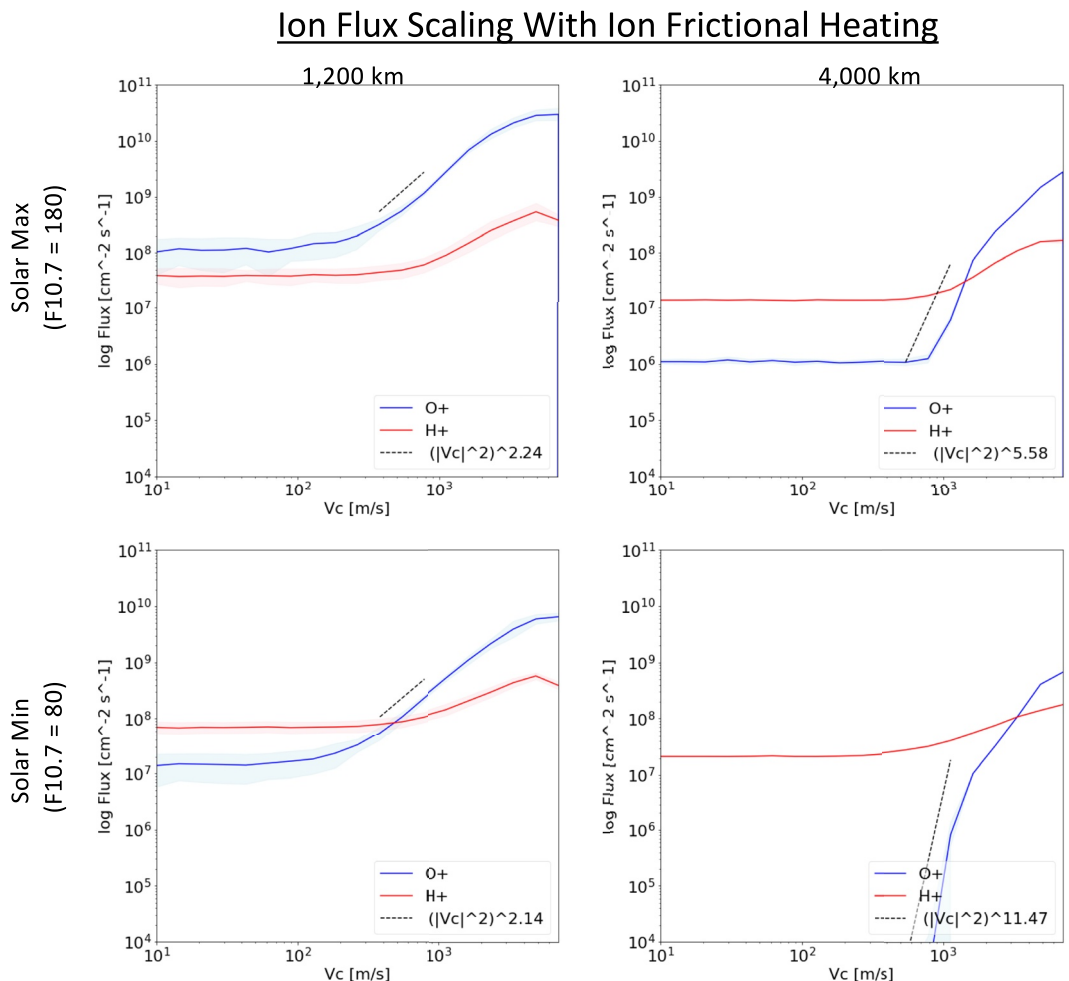


Figure 1. Scaling of ion flux with $V_c = |u_{i\perp} - u_{n\perp}|$ used as a proxy for frictional heating. Results are compared between the top of the exobase transition region at 1,200 km (left column) and 4,000 km typical to FAST observations (right column). Results are also compared between solar maximum (top row) and solar minimum (bottom row).

3.2. Ion Flux Scaling With e^- Precipitation

Soft electron precipitation, or electron precipitation with a mean energy below 1 keV, does not penetrate deeply into the atmosphere. Indeed, most of the energy from this type of precipitation is deposited in the topside F region of the ionosphere where it produces additional ionization, thermal electron heating, and secondary electrons. Therefore, the energy input from soft electron precipitation has been considered an effective method to generate ion upflows (Su et al., 1999). In this section we will look at the scaling of upward ion flux with the energy flux of the soft electron precipitation for the same altitudes and solar EUV inputs as considered in the previous section. We moreover consider two values of characteristic energy (E_o) of the precipitation, $E_o = 100$ and 400 eV.

Figures 2 and 3 present the scaling of the upward O^+ and H^+ flux with the energy flux of electron precipitation for solar minimum and maximum conditions. The format of the figure is the same as Figure 1 discussed in the previous section. As with the frictional heating of the ions, soft electron precipitation can create transient upflows whose peak flux can occur at different times during the simulation. Therefore, we again focus on the peak value of the ion flux regardless at what point in the simulation that flux occurs.

From Figures 2 and 3 we can draw the following conclusions. In general, it is clear that the O^+ responds more strongly than H^+ to the soft electron precipitation. Additionally, the power law dependence is different at low and high altitudes as some of the upward flowing ions at 1,200 km do not have enough energy to reach 4,000 km altitude. The result is a steepening curve connecting ion flux and electron precipitation at higher altitudes. It is

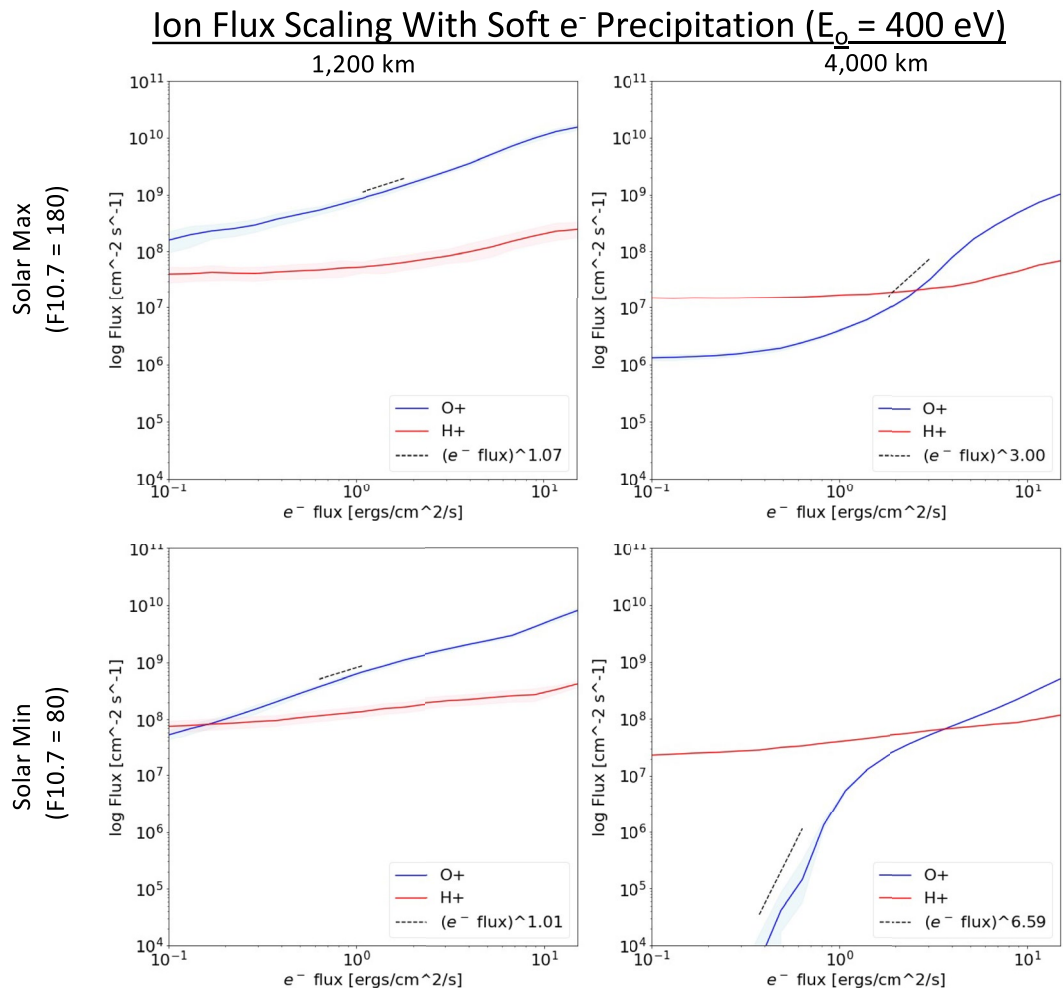


Figure 2. Ion flux scaling with the energy flux of soft electron precipitation with a characteristic energy of 400 eV. The format is the same as Figure 1.

interesting to note that at low altitudes the ion flux increases smoothly without any evidence of a threshold input for the onset of outflow. In contrast, at high altitudes, the O⁺ flux exhibits does exhibit a threshold input. Additionally, the relationship between ion flux and soft electron precipitation is somewhat similar between solar minimum and solar maximum cases, although the magnitude of the peak flux is larger for solar maximum. Finally, we can see that a lower characteristic energy of the soft electron precipitation corresponds to a larger upflow flux. This last point is consistent with the earlier study of Su et al. (1999) who also found that for a fixed energy flux, a lower mean energy of electron precipitation corresponds to greater outflow.

3.3. Ion Flux Scaling With Wave Power

When ions reach higher altitudes they can be further accelerated by various WPI. The heating of ion distributions transverse to the magnetic field by waves can subsequently be converted into organized parallel motion via the mirror force and as a result create very strong upflows and outflows of ions. There are a multitude of waves that can accelerate ions at high altitudes including BBELF waves (Chang et al., 1986), lower hybrid waves (Chang & Coppi, 1981), dispersive Alfvén waves (Chaston et al., 2004), electrostatic ion cyclotron waves (Lysak et al., 1980), among others. A study carried out by André et al. (1998) looking at 200 outflow events seen by the Freja satellite showed that transverse acceleration by BBELF mechanism was the most common type of wave-particle interaction observed. Therefore, in this study we focus primarily on the heating associated with BBELF waves, but we plan to consider other wave modes in future studies.

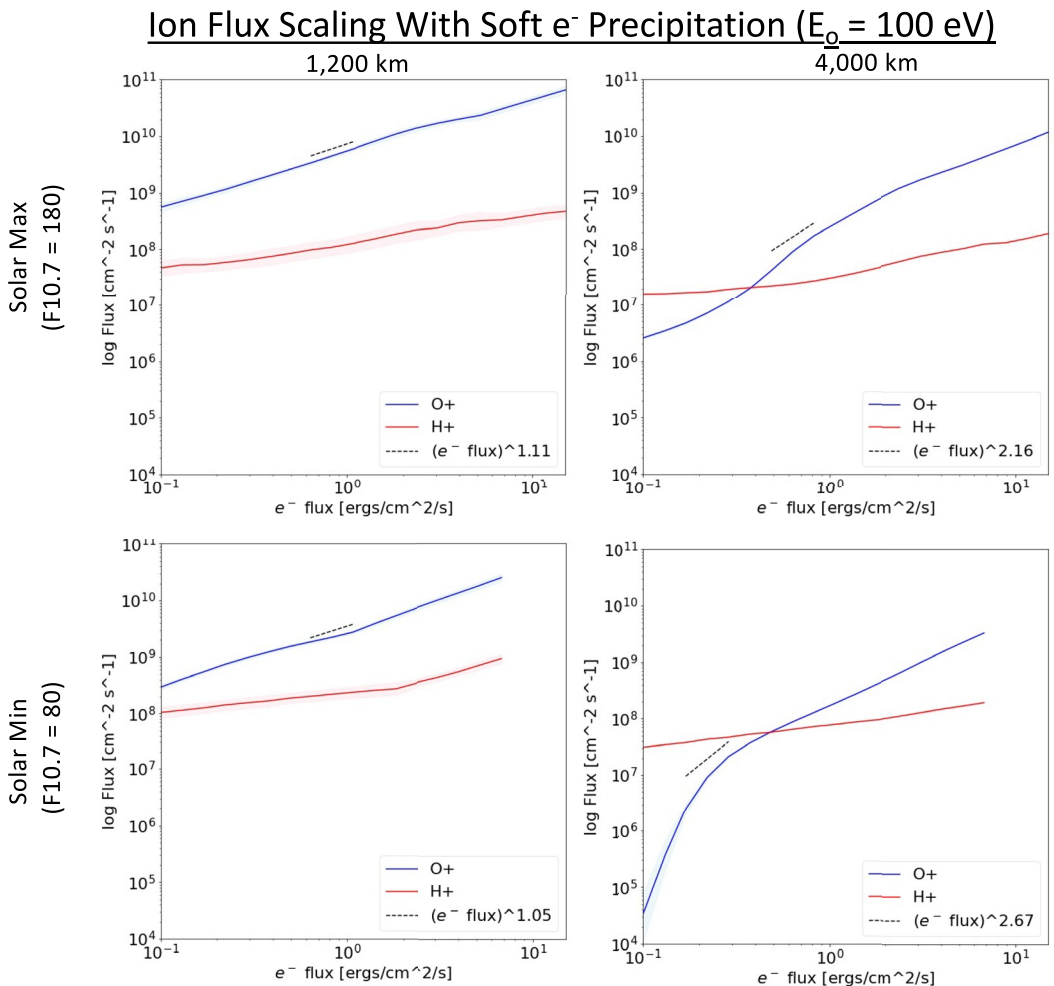


Figure 3. Ion flux scaling with the energy flux of soft electron precipitation with a characteristic energy of 100 eV. The format is the same as Figure 1.

Simulation results showing the relation between upward ion flux and the power spectral density of BBELF waves is presented in Figure 4. As discussed in the introduction, the wave spectrum is defined using a power law. The spectral index α is set to 1.7, and power spectral density is defined at the ion cyclotron frequency at a radial distance of $3 R_e$. That wave spectrum is held constant at 1,000 km and above starting at beginning of the simulation. These parameters are the same as those selected by Zeng and Horwitz (2007). That prior study, however, focused on the steady state solution while our simulation is only 20 min long and is intended to be representative of the physical case of a field line entering the dayside cusp and encountering intense heating for a limited duration. The top row of Figure 4 shows the results for solar maximum conditions while the bottom row shows the results for solar minimum. Additionally, the left column shows the results at the end of the 20 min window, while the right column shows the maximum flux for each value of wave power regardless of where in the simulation it occurred. Additionally, we note that estimates of the limiting flux are included as dashed lines in the plots and will be discussed next.

To better understand Figure 4, we must first discuss the concept of the limiting flux. The limiting flux, or sometimes called the critical flux, represents a theoretical estimate of the maximum ion flux that can be supplied by the ionosphere. Theoretical work on the limiting flux has largely focused on H⁺ and represents the idea that the flux supplied by the ionosphere is limited by the production of H⁺ from the charge exchange reaction of neutral hydrogen with O⁺ (Geisler, 1967). While there are earlier derivations of the limiting flux, a particularly nice derivation is given in Richards and Torr (1985). In their approach, they start with the continuity equation for H⁺ in steady

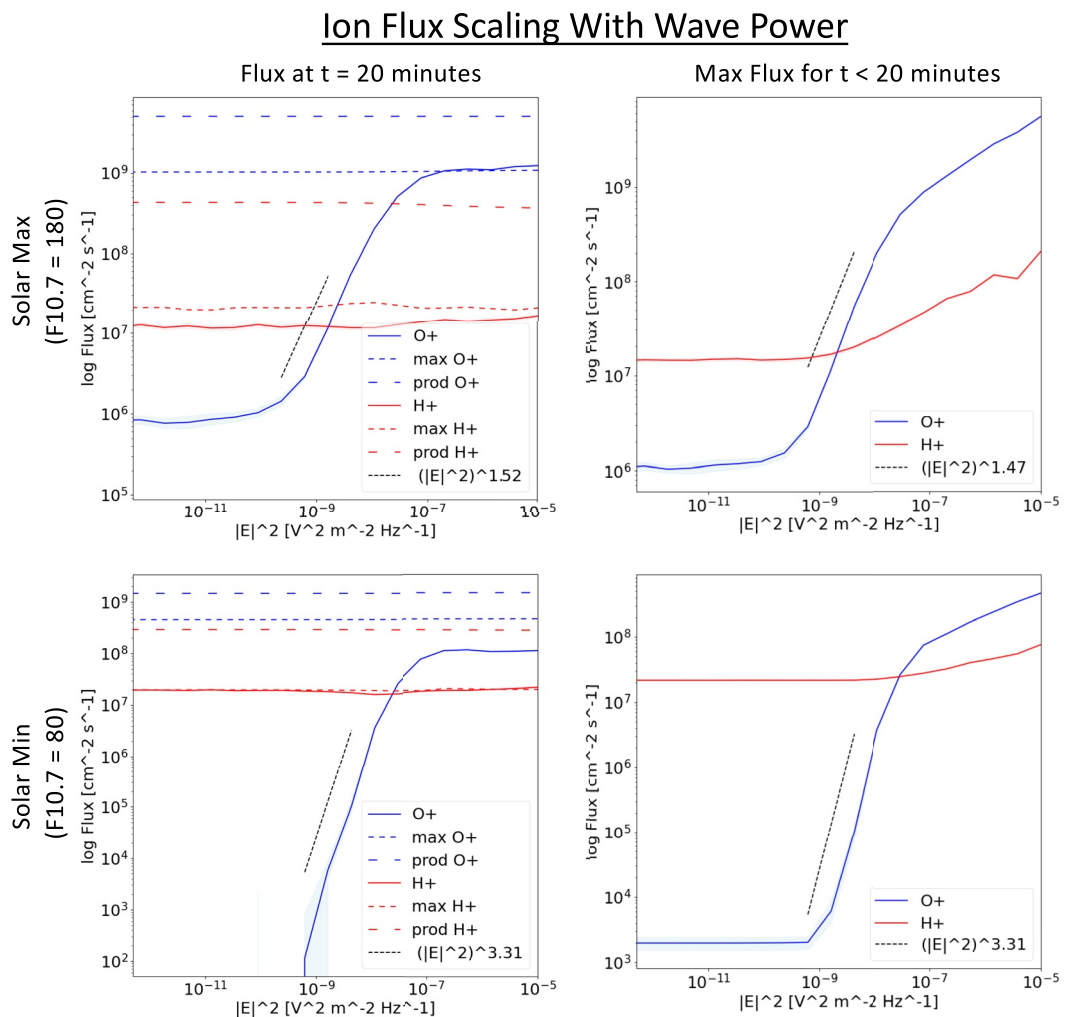


Figure 4. Ion flux at 4,000 km scaling with wave power. Solar maximum conditions are shown on the top row, and solar minimum conditions are shown on the bottom row. The steady state solution are shown in the left column, and the peak flux value over the course of the simulation are shown in the right column. The “max” and “prod” values for each species represent different estimates of the limiting flux defined in the text.

state, and integrate along the magnetic field from an initial position s_o to a position s to obtain an expression for the flux $\phi(s)$ (Richards & Torr, 1985):

$$\phi(s) = \phi_o B(s)/B_o + B_o \int_{s_o}^s \left(P - L - \frac{\partial n}{\partial t} \right) ds / B(s) \quad (5)$$

where $P(s)$ is the production rate for a given ion, $L(s)$ is the loss rate, $B(s)$ is the magnetic field at a point s , and B_o is the magnetic field at the lower boundary s_o . To obtain the limiting flux, they consider a steady state which removes the time derivative, set $\phi_o = 0$ which is a fair approximation at low altitude, set $s = \infty$, and then neglect the loss term in order to find the upper limit of the flux. Following this example, the value of the limiting flux, ϕ_L , at a position, s , along the magnetic field line is given by Richards and Torr (1985):

$$\phi_L = \int_{s_o}^{\infty} P(s) \frac{B_o}{B(s)} ds \quad (6)$$

This equation is identical to Equation 4 of Richards and Torr (1985) once the value of the production rate for H^+ is substituted in for $P(s)$. It is interesting to note that prior to substituting a species specific value for $P(s)$ there are no assumptions in the derivation that limits Equation 6 to H^+ . We can therefore apply the limiting flux concept

equally well to O⁺ by using the production rate for O⁺ in Equation 6. The O⁺ production rate used here includes photoionization, primary electron impact ionization, and secondary electron production which are the dominant terms. For the purposes of this paper, we want to understand the limiting flux from the altitude range that can realistically contribute to ion outflow. Therefore we choose s_o in Equation 6 to be at the location of the peak ion density for each ion. Note that this is also close to the location of peak ion production in our simulation domain.

A rough estimate of the value of the limiting flux in Equation 6 is often found by taking the peak production rate times the scale height, which assumes the integral is dominated by the region around peak production which is assumed to be about one scale height in size. In this paper we will use both estimates of the limiting flux. In Figure 4 the limiting flux calculated from Equation 6 is labeled “prod,” while the limiting flux estimated by taking the peak production times the scale height is labeled “max.” For each case, we scale the limiting flux estimate to 4,000 km for direct comparison to the simulation output at this altitude.

The left hand column of Figure 4 presents the H⁺ and O⁺ ion flux as a function of wave power at 4,000 km altitude together with the limiting flux for solar max and min conditions. These results are taken after a wave-heating duration of 20 min and are close to a steady-state representation of the ion flux in response to wave heating. The limiting flux helps us to understand why the outflow flux saturates. For O⁺, adding more wave power makes a big difference in the amount of flux obtained. As oxygen is 16 times heavier than hydrogen, very little O⁺ flows when wave heating is low, but once a threshold is reached the O⁺ grows as a power law function of the wave intensity. This threshold is the same as the “valve” effect referred to in the earlier work of Zeng and Horwitz (2007). As the wave power is further increased, we reach a point where the ion flux saturates. In other words, no matter how much more wave energy we pump into the simulation, we can not extract any more O⁺ from the ionosphere. Indeed, our O⁺ saturation flux is within 10%–100% of our various estimates of the O⁺ limiting flux, indicating that the saturation is controlled by what the ionosphere can supply. Additionally, comparing the solution for solar min and max we find that both the maximum O⁺ flux, and its power law relationship with wave power, vary with solar cycle.

Comparison of the H⁺ flux at end of the simulation with the estimate of the H⁺ limiting flux is also informative. We see that regardless of wave-power input, the H⁺ is always coming out at values near the limiting flux. Therefore polar wind processes alone are already sufficient to reach the limiting flux the ionosphere can supply and the addition of wave energy will not enhance the steady state flux of H⁺. This result is consistent with past studies. For example, Richards and Torr (1984) notes that the calculations of Raitt et al. (1975) of H⁺ flux into depleted flux tubes are close to the estimated critical flux indicating that polar wind type outflow should be close to these limiting values. Considering the H⁺ and O⁺ flux together, it is therefore clear that the H⁺ polar wind flow defines the lower bound on the out flowing ion flux while the O⁺ limiting flux defines the upper bound. Additionally, as we go from solar maximum to solar minimum the O⁺ limiting flux decreases and the power law slope of the ion flux changes indicating that illumination should be considered when formulating empirical relationships for ion outflow.

Focusing on the near-steady state solution at the end of the simulation can informative, but it can also be misleading as the outflow solution is dynamic. We therefore follow the example of the previous sections and also consider the maximum value of the ion flux regardless of what time in the simulation it occurs. These results are shown in the right hand column of Figure 4. It is interesting to note that for low and moderate wave power the maximum O⁺ flux is quite similar to the value at the end of the simulation; in both cases there is an identical threshold wave power above which the O⁺ flux transitions to a power law, and the power law slope has a similar value. For larger values of wave-heating we start to see bigger differences. A difference of particular note is that the O⁺ and H⁺ flux no longer saturates, although the power law slope for the O⁺ does flatten. In both cases, the peak flux ends up exceeding our estimate of the limiting flux. The idea that our peak fluxes may temporarily exceed the limiting flux may initially be anathema to some readers, but it is important to remember that the limiting flux is a steady state concept and in a dynamic system this value can be temporarily exceeded as a large amount of energy input can lift preexisting ions as well as just newly produced ions. As a consequence, it is possible to see a power law relationship between the H⁺ flux and the wave power, even though the base polar wind flux is already close to the limiting flux value.

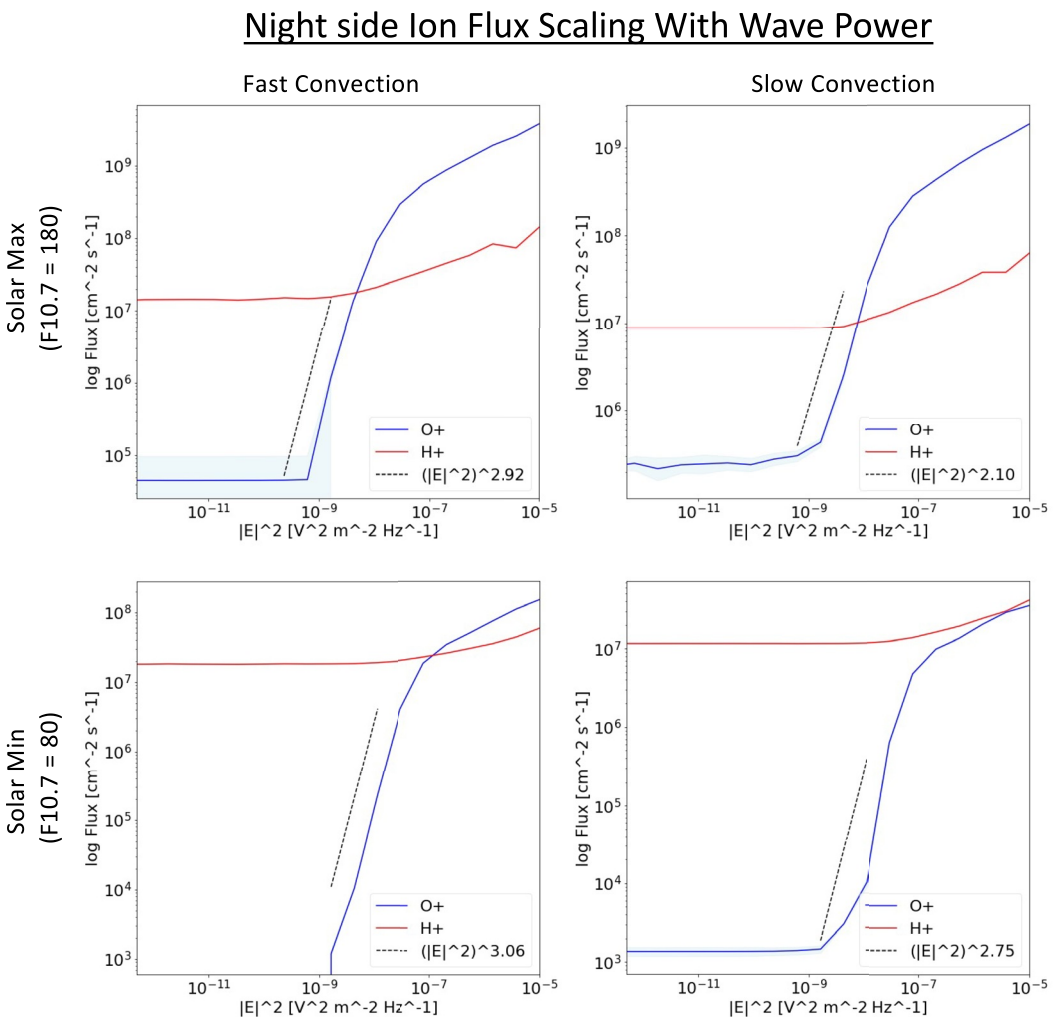


Figure 5. Ion flux at 4,000 km scaling with wave power for nightside conditions. Solar maximum conditions are shown on the top row, and solar minimum conditions are shown on the bottom row. Simulations with fast convection from day to night are shown in the left column, and simulations with slow convection from day to night are shown in the right column.

3.4. Ion Flux Scaling With Wave Power on Nightside

The ion outflow above the nightside auroral region is not the same as the ion outflow above the dayside cusp. Even similar values of wave power input, different ion outflow values should be expected. This is because a field line on the dayside entering the cusp region is full of plasma created from photoionization, whereas a field line on the nightside entering the auroral zone has been in darkness for some time and the plasma on the line is thus depleted. In this section, we consider the ion outflow on a field line entering the nightside auroral zone. The initial condition for these runs is obtained by taking the dayside field line used in the prior sections, and placing it on the nightside for either 834 s or 3,336 s prior to turning on the wave power energy inputs associated with the aurora. These times reflect a convention speed of 2.0 and 0.5 km/s respectively for field line traversing from the terminator to a typical auroral latitude on the nightside.

Figure 5, shows the ion outflow scaling with wave power for a field line entering the nightside auroral region. Cases are shown for solar max and solar min, as well as for a fast and slowly convecting field line. We find that the power law slope is somewhat larger for the fast convection and peak flux values are also larger. This is because less of the plasma on the field line has been lost in the traverse from the terminator to the polar cap. Therefore more plasma is available on the field line upon reaching the aurora for acceleration by the waves. Similar to prior sections, differences in the solar flux between solar min and max, manifest in the peak flux, power law slope, and

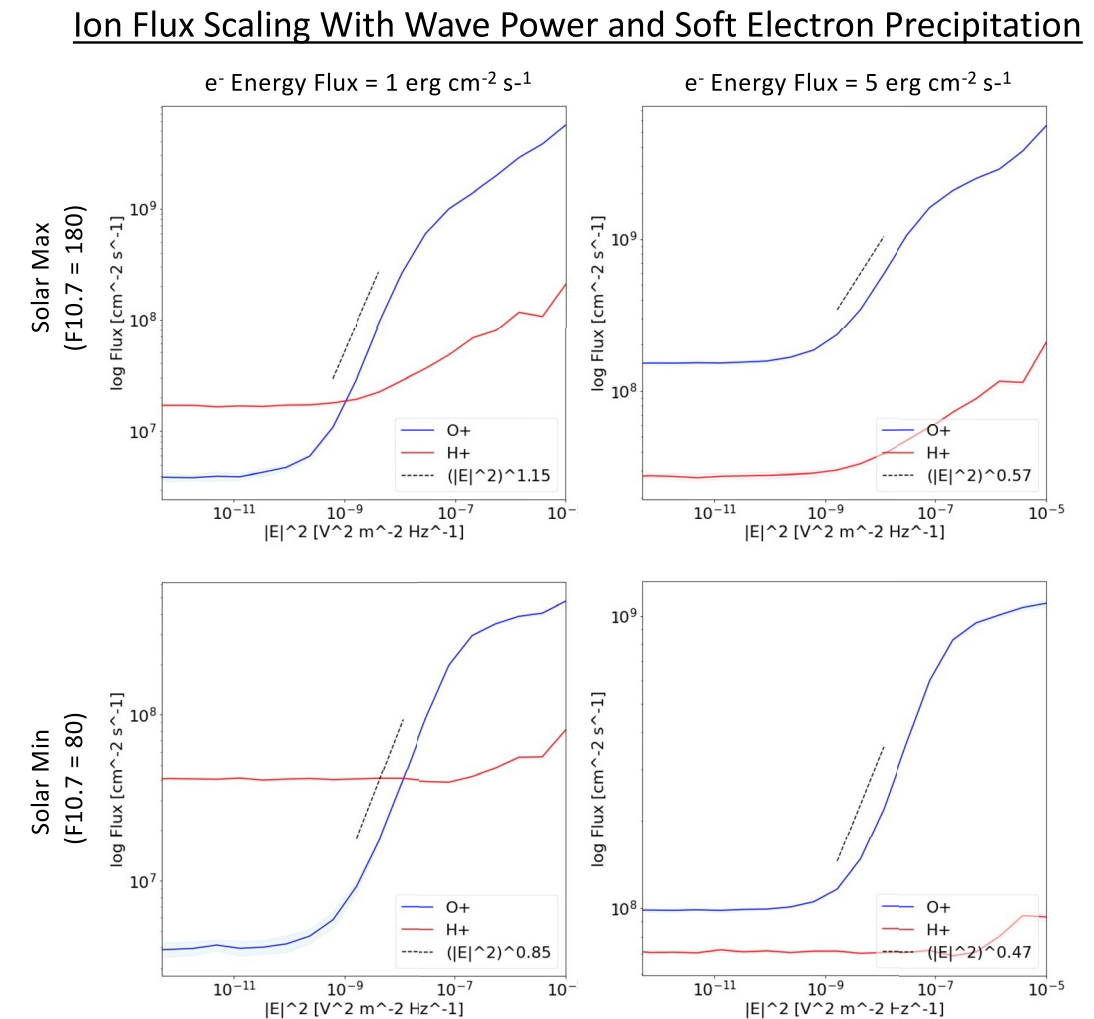


Figure 6. Ion flux at 4,000 km scaling with wave power when electron precipitation is present. We consider precipitation with a characteristic energy of 100 eV and an energy flux of $1 \text{ erg cm}^{-2} \text{s}^{-1}$ (left column) and $5 \text{ erg cm}^{-2} \text{s}^{-1}$ (right column). As in prior figures, solar maximum conditions are shown on the top row, and solar minimum conditions are shown on the bottom row.

composition mix of the outflowing ions. In particular, we see that the outflow is more O^+ rich at solar max and more flux is obtained.

3.5. Ion Flux Scaling With e^- Precipitation and Wave Power Present

One of the difficulties in understanding how energy inputs are connected to ion outflow, is that often times outflows are observed with multiple energy inputs simultaneously. As noted in Strangeway et al. (2005), many of the energy inputs that are correlated with ion outflow are also correlated with each other. This ambiguity makes it difficult ascertain causality, or understand the relative contributions of each energy input. In the prior sections, each energy input was evaluated in isolation, but this section we will consider two energy inputs simultaneously: wave heating and soft electron precipitation.

Figure 6 presents the results of our simulations on how the ion flux scales with wave power when soft electron precipitation is also present. These results present a modest amount of soft electron energy flux of $1 \text{ erg cm}^{-2} \text{s}^{-1}$ (left column) and a more intense value of $5 \text{ erg cm}^{-2} \text{s}^{-1}$ (right column). Both cases assume the characteristic energy of the soft electron precipitation is 400 eV. We also consider the result for solar max (top row) and solar min (bottom row). As in prior sections, we focus on the peak outflow flux during the simulation.

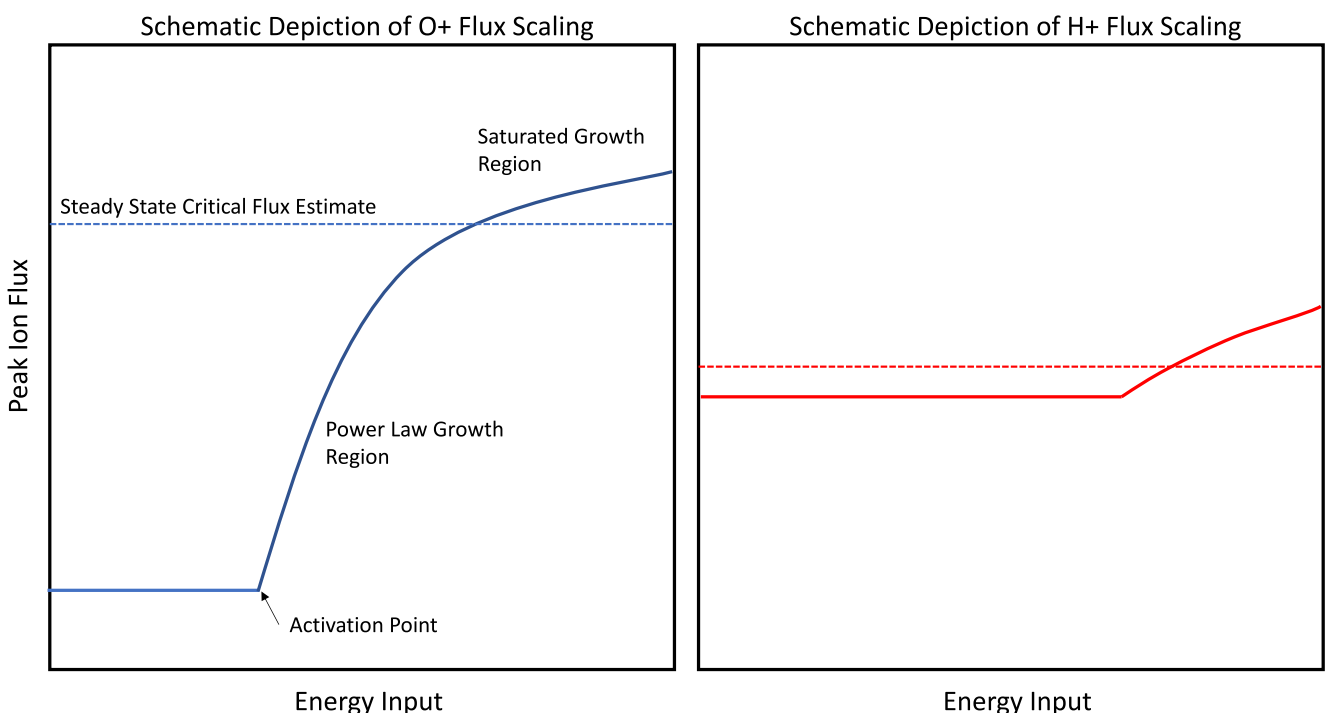


Figure 7. A schematic depiction of the response of ion flux to energy input.

We find that the simultaneous presence of soft electron precipitation can significantly change the relationship between wave power and upward ion flux. Specifically the inclusion of soft electron precipitation results in more O^+ flux for a given amount of wave heating. We also find that the relative composition and power law response of the ion flux to wave power is significantly different when this electron precipitation is included. The difference is particularly pronounced for solar minimum conditions and for stronger values of electron energy flux. The reason that a strong difference is seen for solar minimum is that these conditions have a reduced contribution from the solar ionizing flux. Therefore the addition of soft electron precipitation increases the available supply of plasma relatively more than for solar maximum and thus creates a greater impact on the resulting ion flux. Similarly, as you increase the energy flux of the precipitation you also increase the ionization and hence the supply of plasma relative to the solar EUV flux contribution for both solar maximum and solar minimum. An important takeaway from these results is that scaling relationships between ion flux and energy inputs can change dramatically when multiple inputs occur simultaneously.

4. Discussion and Conclusions

In this study we examined the scaling of ion upflow and outflow with different energy input using numerical simulation. The energy inputs examined included the frictional heating the ions due to ion convection relative to the neutrals, soft electron precipitation, and wave particle interactions. These quantities were chosen to align with the parameters explored by past observational studies. We further explored how the response of ion flux to energy input is affected by solar illumination by considering solar minimum and maximum conditions, as well as day-night differences for some select cases. We will now summarize and discuss some of the main conclusions of the study.

In discussing the results it is useful to introduce a schematic illustration of the ion flux response to a generic energy input. Such a representation is provided in Figure 7 for O^+ (left) and H^+ (right). In general, the O^+ flux starts at a low value far below the limiting flux, whereas we found that the H^+ flux comes out close to the limiting flux which is consistent with past studies (Raitt et al., 1975; Richards & Torr, 1984). As the energy input increases many of our simulations found that there is an “activation point” where the flux starts to increase sharply. This point can be different for each ion species and is similar to the “valve” effect identified in the simulations of

Zeng and Horwitz (2007). Once the activation energy is reached, the ion flux grows with a power law until the critical flux is approached. After this point the growth rate of the peak flux with energy input dramatically slows as we enter a saturated growth regime. In the following discussion we will allude to this schematic picture when summarizing our conclusions.

When looking at the low altitude acceleration processes we find some interesting conclusions. In the case of frictional heating of the ions, we found that H⁺ and O⁺ have different activation points for showing a response in the ion flux to the convection velocity that drives the heating. The activation point for O⁺ is found to occur at a lower convection velocity than for H⁺. In contrast, there is no sign of an activation point at low altitudes for the case of soft electron precipitation. There is instead a smooth increase in peak ion flux with energy. However, an activation point does become visible at higher altitudes. It is also clear that O⁺ responds more strongly than H⁺ to frictional heating and hence DC Poynting flux. This result is consistent with the study of Zhao et al. (2020). However, we find that O⁺ also responds more strongly than H⁺ to soft electron precipitation which is inconsistent. As we will discuss more shortly, illumination is also found to be important in defining the maximum ion flux that can be extracted. In general, a greater ion supply at solar maximum meaning that more ions are available to be lifted which lifts the critical flux and raises flux in the saturated growth regime.

In this study we also examined ion scaling with wave power, focusing on the ICRH mechanisms. When looking at steady state solutions it is clear that there is a minimum outflow defined by the H⁺ polar wind which does not substantially change as wave power increases. We note however that the O⁺ flux can set the floor on the outflow when significant soft electron precipitation is present at the same time as the waves. A maximum outflow is also seen which agrees qualitatively with estimates of the O⁺ limiting flux. Looking at the steady solution is similar to what has been done in the past by Zeng and Horwitz (2007). No saturation growth regime is visible in the steady state as ion flux ceases to grow with additional energy input. However, when we look at the peak outflow instead of steady state, it is found that the flux does not saturate. Instead, the limiting flux can be temporarily exceeded, and a response is now visible in the H⁺. We also see a clear saturation growth regime where at large wave power input the peak ion flux will continue to grow, but at a reduced rate. As outflow is by definition a time depended processes and not steady state, it is important to consider such effects when understanding data which could be taken at any stage of outflow formation.

The level of illumination is also found to play an important role in all the studies we examined. When comparing the simulations done under solar maximum and solar minimum conditions, we find that the peak ion flux is higher under solar maximum conditions. Additionally, the relative ion composition is impacted, and the input level for which the ion flux changes from mostly H⁺ to mostly O⁺ moves to a lower value. These changes are true for all energy input types considered. Similarly, the relation between ion flux and wave power the nightside is found to be different than on the dayside, particularly for solar minimum conditions with some dependence on the convection speed by which the dayside flux tube is transported to the nightside acceleration region. This study did not examine how the solar zenith angle (SZA) will impact the ion outflow, however the recent study by Kitamura et al. (2021) analyzed FAST satellite data and found little impact of SZA. However, Kitamura et al. (2021) did find that illumination plays an important role with most large outflows observed on the dayside. Clearly solar illumination conditions should be considered when trying to understand the connection between ion flux and energy inputs that drive that flux.

One of the limitations of the present study is that the thermosphere is being modeled as an unchanging empirical background without changing in response to the applied forcing. This imposes some limitation on our results. First, it is likely that the MSIS temperature does not represent the true thermospheric neutral temperature for cases of strong frictional heating. To estimate the magnitude of the error consider the equilibrium ion temperature during a frictional heating event (Thayer and Semeter (2004), Equation A.15)

$$T_i = T_n + \frac{m_n}{3k_B} \|\mathbf{u}_i - \mathbf{u}_n\|^2 \quad (7)$$

$$= T_n^{MSIS} + (T_n - T_n^{MSIS}) + \frac{m_n}{3k} \|\mathbf{u}_i - \mathbf{u}_n\|^2 \quad (8)$$

By using MSIS for the neutral temperature we are likely underestimating T_i by approximately $(T_n - T_n^{MSIS})$. This will likely influence the ion flux although the magnitude of the effect is difficult to estimate. Using MSIS for the neutral atmosphere in the cases of soft electron precipitation in the cusp has the effect of missing the changes

in the altitudinal distribution of Joule heating associated with the changing altitudinal distribution of Pedersen conductivity. This means we ignore the impact of this effect on the neutral temperature and on the cusp neutral upwelling (e.g., Deng et al., 2013; Zhang et al., 2015). Note that the present results only consider the net difference between the ion and neutral horizontal winds, but do not consider the vertical winds. As discussed here, the impact of a dynamic thermosphere on ion outflow is likely important is a limitation of the present study which should be considered in future work.

Many studies attempting to connect ion outflow with energy inputs typically consider the ion flux's variation with one energy input at a time. In observational studies (e.g., Strangeway et al., 2005; Zheng et al., 2005) it is common to present ion flux plotted against energy inputs such as Poynting Flux or electron precipitation, and then fit a power law line through the data points. However, there is often a large amount of scatter around these lines making it hard to interpret the results. One plausible explanation for this scatter is the fact that energy inputs connected with ion outflow are often also correlated with each other (Strangeway et al., 2005). Therefore a curve representing ion outflow with wave power that does not include precipitation, can look quite different from data that also includes varying amounts of soft electron precipitation of varying characteristics. Indeed, we found in our simulations that the connection between ion flux and wave power does look quite different when significant levels soft electrons precipitation is included. The curves can have quite different power law growth and different saturation growth regimes. This is particularly true for solar minimum conditions where the contribution of impact ionization is proportionally greater than the photoionization as compared to solar maximum. Interestingly, the minimum ion flux in these cases can set by the O⁺ flux if significant soft electron precipitation is occurring. We therefore conclude that relations between ion flux and energy inputs should account for all energy inputs, including the solar illumination conditions.

Data Availability Statement

The model output data used in production of all figures has been made available online for download at <https://doi.org/10.5281/zenodo.6527337>.

Acknowledgments

A. Glocer and L. K. S. Daldorff acknowledge support from NASA (17-SSW17-0063 and 19-HFORT19-2-0021). Resources supporting this work were provided by the NASA High-End Computing (HEC) Program through the NASA Advanced Supercomputing (NAS) Division at Ames Research Center. All modeling tools described in publication are available online through the Space Weather Modeling Framework. The authors would like to acknowledge useful discussions facilitated by the Helio-physics MACH DRIVE phase 1 center. The authors would also like to thank S. Solomon for making the GLOW model available.

References

- André, M., Norqvist, P., Andersson, L., Eliasson, L., Eriksson, A. I., Blomberg, L., et al. (1998). Ion energization mechanisms at 1700 km in the auroral region. *Journal of Geophysical Research*, 103(A3), 4199–4222. <https://doi.org/10.1029/97JA00855>
- Barakat, A. R., & Schunk, R. W. (2001). Effects of wave-particle interactions on the dynamic behavior of the generalized polar wind. *Journal of Atmospheric and Solar-Terrestrial Physics*, 63(1), 75–83. [https://doi.org/10.1016/S1364-6826\(00\)00106-1](https://doi.org/10.1016/S1364-6826(00)00106-1)
- Brambles, O. J., Lotko, W., Zhang, B., Wiltberger, M., Lyon, J., & Strangeway, R. J. (2011). Magnetosphere sawtooth oscillations induced by ionospheric outflow. *Science*, 332(6034), 1183–1186. <https://doi.org/10.1126/science.1202869>
- Chang, T., & Coppi, B. (1981). Lower hybrid acceleration and ion evolution in the supraauroral region. *Geophysical Research Letters*, 8(12), 1253–1256. <https://doi.org/10.1029/GL008i012p01253>
- Chang, T., Crew, G. B., Hershkowitz, N., Jasperse, J. R., Retterer, J. M., & Winningham, J. D. (1986). Transverse acceleration of oxygen ions by electromagnetic ion cyclotron resonance with broad band left-hand polarized waves. *Geophysical Research Letters*, 13(7), 636–639. <https://doi.org/10.1029/GL013i007p00636>
- Chappell, C. R., Moore, T. E., & Waite, J. H. (1987). The ionosphere as a fully adequate source of plasma for the earth's magnetosphere. *Journal of Geophysical Research*, 92(A6), 5896–5910. <https://doi.org/10.1029/ja092ia06p05896>
- Chaston, C. C., Bonnell, J. W., Carlson, C. W., McFadden, J. P., Ergun, R. E., Strangeway, R. J., & Lund, E. J. (2004). Auroral ion acceleration in dispersive Alfvén waves. *Journal of Geophysical Research*, 109(A4), A04205. <https://doi.org/10.1029/2003JA010053>
- Chaston, C. C., Carlson, C. W., McFadden, J. P., Ergun, R. E., & Strangeway, R. J. (2007). How important are dispersive Alfvén waves for auroral particle acceleration? *Geophysical Research Letters*, 34(7), L07101. <https://doi.org/10.1029/2006GL029144>
- Crew, G. B., Chang, T., Retterer, J. M., Peterson, W. K., Gurnett, D. A., & Huff, R. L. (1990). Ion cyclotron resonance heated conics—Theory and observations. *Journal of Geophysical Research*, 95(A4), 3959. <https://doi.org/10.1029/ja095ia04p03959>
- Deng, Y., Fuller-Rowell, T. J., Ridley, A. J., Knipp, D., & Lopez, R. E. (2013). Theoretical study: Influence of different energy sources on the cusp neutral density enhancement. *Journal of Geophysical Research: Space Physics*, 118(5), 2340–2349. <https://doi.org/10.1002/jgra.50197>
- Garcia, K. S., Merkin, V. G., & Hughes, W. J. (2010). Effects of nightside O⁺ outflow on magnetospheric dynamics: Results of multifluid MHD modeling. *Journal of Geophysical Research*, 115(A12), A00J09. <https://doi.org/10.1029/2010JA015730>
- Geisler, J. E. (1967). On the limiting daytime flux of ionization into the protonosphere. *Journal of Geophysical Research*, 72(1), 81–85. <https://doi.org/10.1029/JZ072i001p00081>
- Glocer, A., Gombosi, T. I., Toth, G., Hansen, K. C., Ridley, A. J., & Nagy, A. (2007). Polar wind outflow model: Saturn results. *Journal of Geophysical Research*, 112(A1), A01304. <https://doi.org/10.1029/2006JA011755>
- Glocer, A., Khazanov, G., & Liemohn, M. (2017). Photoelectrons in the quiet polar wind. *Journal of Geophysical Research: Space Physics*, 122(6), 6708–6726. <https://doi.org/10.1002/2017JA024177>
- Glocer, A., Toth, G., & Fok, M.-C. (2018). Including kinetic ion effects in the coupled global ionospheric outflow solution. *Journal of Geophysical Research: Space Physics*, 123(4), 2851–2871. <https://doi.org/10.1002/2018JA025241>
- Glocer, A., Toth, G., Gombosi, T., & Welling, D. (2009). Modeling ionospheric outflows and their impact on the magnetosphere, initial results. *Journal of Geophysical Research*, 114, A05216. <https://doi.org/10.1029/2009JA014053>

- Gombosi, T. I., & Killeen, T. L. (1987). Effects of thermospheric motions on the polar wind: A time-dependent numerical study. *Journal of Geophysical Research*, 92(A5), 4725–4729. <https://doi.org/10.1029/ja092ia05p04725>
- Gombosi, T. I., & Nagy, A. (1989). Time-dependent modeling of field aligned current-generated ion transients in the polar wind. *Journal of Geophysical Research*, 94(A1), 359–369. <https://doi.org/10.1029/ja094ia01p00359>
- Huddleston, M. M., Chappell, C. R., Delcourt, D. C., Moore, T. E., Giles, B. L., & Chandler, M. O. (2005). An examination of the process and magnitude of ionospheric plasma supply to the magnetosphere. *Journal of Geophysical Research*, 110(A9), 12202. <https://doi.org/10.1029/2004JA010401>
- Karimabadi, H., Roytershteyn, V., Mouikis, C., Kistler, L., & Daughton, W. (2011). Flushing effect in reconnection: Effects of minority species of oxygen ions. *Planetary and Space Science*, 59(7), 526–536. <https://doi.org/10.1016/j.pss.2010.07.014>
- Khazanov, G. V., Liemohn, M. W., & Moore, T. E. (1997). Photoelectron effects on the self-consistent potential in the collisionless polar wind. *Journal of Geophysical Research*, 102(A4), 7509–7522. <https://doi.org/10.1029/96JA03343>
- Killeen, T., & Roble, R. (1984). An analysis of the high-latitude thermospheric wind pattern calculated by a thermospheric general circulation model 1. Momentum forcing. *Journal of Geophysical Research*, 89(A9), 7509–7522. <https://doi.org/10.1029/ja089ia09p07509>
- Kitamura, N., Seki, K., Keika, K., Nishimura, Y., Hori, T., Hirahara, M., et al. (2021). On the relationship between energy input to the ionosphere and the ion outflow flux under different solar zenith angles. *Earth Planets and Space*, 73(1), 1–20. <https://doi.org/10.1186/s40623-021-01532-y>
- Lennartsson, W., Sharp, R. D., Shelley, E. G., Johnson, R. G., & Balsiger, H. (1981). Ion composition and energy distribution during 10 magnetic storms. *Journal of Geophysical Research*, 86(A6), 4628–4638. <https://doi.org/10.1029/JA086iA06p04628>
- Lin, M.-Y., Ilie, R., & Glocer, A. (2020). The contribution of N^+ ions to earth's polar wind. *Geophysical Research Letters*, 47(18), e2020GL089321. <https://doi.org/10.1029/2020GL089321>
- Lysak, R., Hudson, M., & Temerin, M. (1980). Ion heating by strong electrostatic ion cyclotron turbulence. *Journal of Geophysical Research*, 85(A2), 678–686. <https://doi.org/10.1029/JA085iA02p00678>
- Moore, T. E., Fok, M.-C., Chandler, M. O., Chappell, C. R., Christon, S. P., Delcourt, D. C., et al. (2005). Plasma sheet and (nonstorm) ring current formation from solar and polar wind sources. *Journal of Geophysical Research*, 110(A2), A02210. <https://doi.org/10.1029/2004JA010563>
- Picone, J. M., Hedin, A. E., Drob, D. P., & Aikin, A. C. (2002). NRLMSISE-00 empirical model of the atmosphere: Statistical comparisons and scientific issues. *Journal of Geophysical Research*, 107(A12), SIA15-1–SIA15-16. <https://doi.org/10.1029/2002ja009430>
- Raitt, W., Schunk, R., & Banks, P. (1975). A comparison of the temperature and density structure in high and low speed thermal proton flows. *Planetary and Space Science*, 23(7), 1103–1117. [https://doi.org/10.1016/0032-0633\(75\)90200-7](https://doi.org/10.1016/0032-0633(75)90200-7)
- Rees, M. H. (1989). The interaction of energetic electrons and ions with the upper atmosphere. In *Cambridge atmospheric and space science series* (pp. 24–56). Cambridge University Press. <https://doi.org/10.1017/CBO9780511573118.004>
- Retterer, J. M., Chang, T., & Jasperse, J. R. (1994). Transversely accelerated ions in the topside ionosphere. *Journal of Geophysical Research*, 99(A7), 13189–13201. <https://doi.org/10.1029/93JA03570>
- Richards, P. G., & Torr, D. (1984). An investigation of the consistency of the ionospheric measurements of the photoelectron flux and solar EUV flux. *Journal of Geophysical Research*, 89(A7), 5625. <https://doi.org/10.1029/ja089ia07p05625>
- Richards, P. G., & Torr, D. G. (1985). Seasonal, diurnal, and solar cyclical variations of the limiting H^+ flux in the earth's topside ionosphere. *Journal of Geophysical Research*, 90(A6), 5261–5268. <https://doi.org/10.1029/JA090iA06p05261>
- Richards, P. G., & Torr, D. G. (1986). A factor of 2 reduction in theoretical F_2 peak electron density due to enhanced vibrationally excitation of N_2 in summer at solar maximum. *Journal of Geophysical Research*, 91(A10), 11331. <https://doi.org/10.1029/ja091ia10p11331>
- Schunk, R. W., & Nagy, A. F. (2000). *Ionospheres: Physics, plasma physics, and chemistry*. Cambridge University Press.
- Seo, Y., Horwitz, J. L., & Caton, R. (1997). Statistical relationships between high-latitude ionospheric F region/topside upflows and their drivers: DE 2 observations. *Journal of Geophysical Research*, 102(A4), 7493–7500. <https://doi.org/10.1029/97JA00151>
- Shay, M. A., Drake, J. F., Swisdak, M., & Rogers, B. N. (2004). The scaling of embedded collisionless reconnection. *Physics of Plasmas*, 11(5), 2199–2213. <https://doi.org/10.1063/1.1705650>
- Solomon, S. C. (2017). Global modeling of thermospheric airglow in the far ultraviolet. *Journal of Geophysical Research: Space Physics*, 122(7), 7834–7848. <https://doi.org/10.1002/2017JA024314>
- Solomon, S. C., Hays, P. B., & Abreu, V. J. (1988). The auroral 6300 Å emission: Observations and modeling. *Journal of Geophysical Research*, 93(A9), 9867–9882. <https://doi.org/10.1029/JA093iA09p09867>
- Strangeway, R. J. (2012). The equivalence of joule dissipation and frictional heating in the collisional ionosphere. *Journal of Geophysical Research*, 117(A2), A02310. <https://doi.org/10.1029/2011JA017302>
- Strangeway, R. J., Ergun, R. E., Su, Y.-J., Carlson, C. W., & Elphic, R. C. (2005). Factors controlling ionospheric outflows as observed at intermediate altitudes. *Journal of Geophysical Research*, 110(A9), 3221. <https://doi.org/10.1029/2004JA010829>
- Su, Y.-J., Caton, R. G., Horwitz, J. L., & Richards, P. G. (1999). Systematic modeling of soft-electron precipitation effects on high-latitude F region and topside ionospheric upflows. *Journal of Geophysical Research*, 104(A1), 153–163. <https://doi.org/10.1029/1998JA900068>
- Thayer, J. P., & Semeter, J. (2004). The convergence of magnetospheric energy flux in the polar atmosphere. *Journal of Atmospheric and Solar-Terrestrial Physics*, 66(10), 807–824. <https://doi.org/10.1016/j.jastp.2004.01.035>
- Welling, D. T., Jordanova, V. K., Zaharia, S. G., Glocer, A., & Toth, G. (2011). The effects of dynamic ionospheric outflow on the ring current. *Journal of Geophysical Research*, 116(A15), A00119. <https://doi.org/10.1029/2010JA015642>
- Zeng, W., & Horwitz, J. L. (2007). Formula representation of auroral ionospheric O^+ outflows based on systematic simulations with effects of soft electron precipitation and transverse ion heating. *Geophysical Research Letters*, 34(6), L06103. <https://doi.org/10.1029/2006GL028632>
- Zhang, B., Lotko, W., Brambles, O., Wiltberger, M., & Lyon, J. (2015). Electron precipitation models in global magnetosphere simulations. *Journal of Geophysical Research: Space Physics*, 120(2), 1035–1056. <https://doi.org/10.1002/2014JA020615>
- Zhao, K., Kistler, L. M., Lund, E. J., Nowrouzi, N., Kitamura, N., & Strangeway, R. J. (2020). Factors controlling O^+ and H^+ outflow in the cusp during a geomagnetic storm: FAST/TEAMS observations. *Geophysical Research Letters*, 47(11), e2020GL086975. <https://doi.org/10.1029/2020GL086975>
- Zheng, Y., Moore, T. E., Mozer, F. S., Russell, C. T., & Strangeway, R. J. (2005). Polar study of ionospheric ion outflow versus energy input. *Journal of Geophysical Research*, 110(A9), 7210. <https://doi.org/10.1029/2004JA010995>